

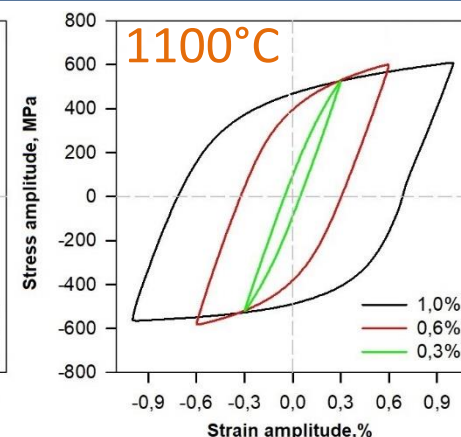
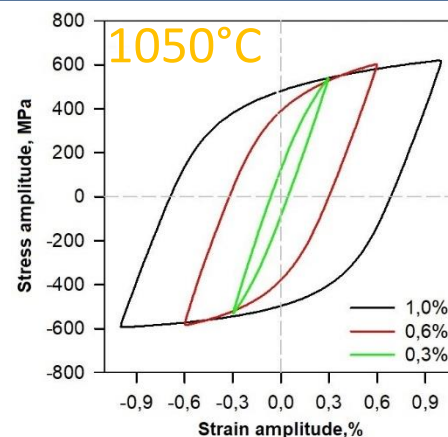
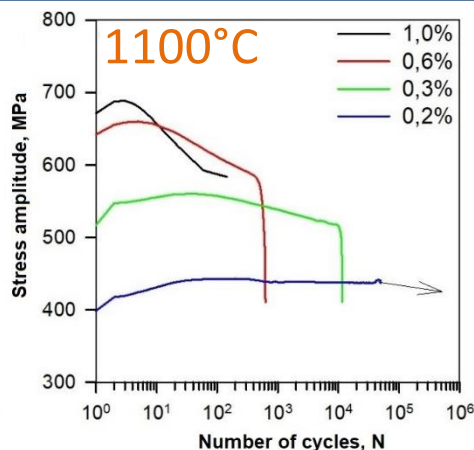
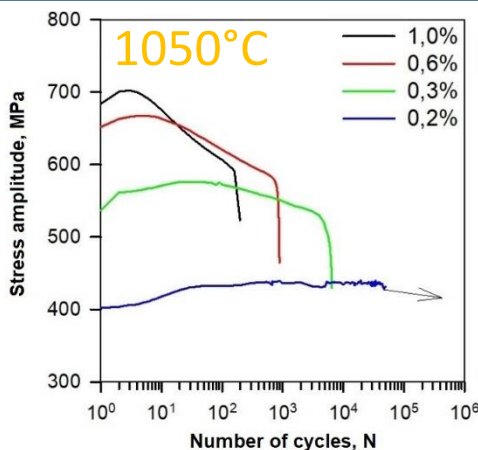
brazhnikov@bsu.edu.ru

EFFECT OF QUENCHING TEMPERATURE ON LOW-CYCLE FATIGUE AT ROOM TEMPERATURE OF 10%CR STEEL WITH HIGH BORON CONTENT

Brazhnikov I.S., Fedoseeva A.E.

Belgorod State National Research University, Belgorod, Russia

High-chromium steels are a promising material for the manufacture of power plant components that will operate at ultra-supercritical steam parameters (temperature 600–620 °C, pressure 25–30 MPa). At present, there is a transition to ultra-supercritical steam parameters, which will increase the efficiency of power plants to 45%. Ingots of 10%Cr-3%Co-2W-0.5Mo-0.8Cu-0.2Re-0.003N-0.01B steel were homogenized at 1200°C for 16 h. Heat treatment of the steel included normalization at 1050°C or 1100°C for 1 h and tempering at 770°C for 3 h.



With amplitude of 0.2% for two quenching temperatures, the number of cycles before failure exceeds the conventional low-cycle fatigue (LCF) threshold of 50 thousand cycles, and a decision was made to stop testing before the sample failed.

Hysteresis loops have an asymmetry that increases as the size of the deformation increases. The asymmetry of the loop is associated with the Bauschinger effect: the wider the loop, the greater the Bauschinger deformation

Temperature, °C	Strain amplitude, %	0,3	0,6	1
1050	Dislocation density, $\times 10^{14} \text{ m}^{-2}$	1,9±0,2	1,6±0,7	4,6±1,6
	Lath width, nm	385±25	405±25	410±25
1100	Dislocation density, $\times 10^{14} \text{ m}^{-2}$	3,3±0,6	2,5±0,9	1,7±0,8
	Lath width, nm	360±25	360±25	390±30

After the LCF test at room temperature, the structure of the tempered martensitic lath structure is preserved, and the transformation of the laths into subgrains does not occur. The dislocation density after the LCF test changes at the error level, and no dependence on the deformation amplitude is observed. The width of the laths increases slightly.

Conclusion

The greatest difference in the number of cycles to failure between two different heat treatments is observed at a deformation amplitude of 0.3%. Increasing the deformation amplitude from 0.3 to 1% leads to a decrease in the number of cycles to failure by 2 orders of magnitude. The steel under study retains the tempered troostite structure and does not transform from lath to subgrain. In general, no significant differences were observed between the two quenching temperatures when tested at LCF.

CRACKING BEHAVIOUR OF NIKEL-BASED SUPERALLOY DURING DIRECT LASER DESPOSITION

Ilya Astakhov^{1,2}, Margarita Klimova^{1,2*}, Anastasiia Dmitrieva¹, Rudolf Korsmik¹, Grigoriy Zadykyan¹, Nikita Yurchenko^{1,2}, Sergey Zherebtsov^{1,2}, Nikita Stepanov^{1,2}, Olga Klimova-Korsmik¹

¹World-Class Research Center, "Advanced Digital Technologies", State Marine Technical University, 190121 Saint Petersburg, Russia

²Laboratory of Bulk Nanostructured Materials, Belgorod State University, Belgorod, Russia

Today nickel-based superalloys are actively used in the aviation, power and shipbuilding industries and are the main materials for the production of engine components operating at elevated temperatures. However, the production of complex-shaped parts using traditional methods such as casting, directional crystallization and powder metallurgy often requires subsequent deformation and heat treatment, which complicates the production process. Additive manufacturing (AM) of nickel-based alloys, namely direct laser deposition (DLD), allows for the production of large-sized parts or the repair of critical components with the requisite surface quality and desired mechanical properties. However, it is widely known that nickel-based superalloys containing a high fraction of strengthening γ' phase are highly susceptible to cracking during AM processes.

In this work, the effect of deposition mode parameters on the microstructure, mechanical properties and cracking behavior of the nickel-based superalloy was investigated. Two thin walls were fabricated by DLD under different conditions. The results of the alloy microstructure study demonstrated successful fabrication of crack-free wall at a low-energy process with power of 200 W, and a scanning speed of 3 mm/s. At the same time, increasing the energy input to 1800 W power and 10 mm/s scanning speed resulted in the development of two types of cracks: solidification hot cracking and ductility-dip cracking caused by σ -phase particles. The microstructure of the crack-free wall consisted predominantly of fine equiaxed grains with an average size of $\sim 19 \mu\text{m}$, while in the cracked wall the epitaxial grain growth led to the formation of a coarse columnar structure with long, straight high-angle boundaries, that provide more possibilities for fast crack propagation.

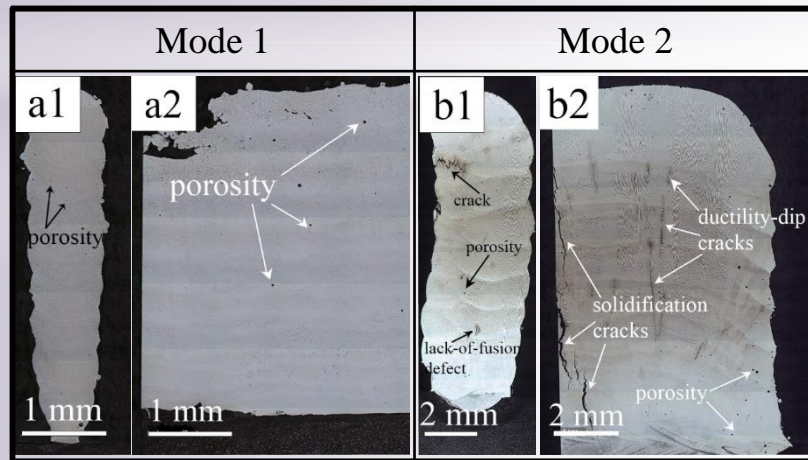


Figure 1. Overall view of the crack-free (Mode 1) and cracked (Mode 2) walls and macrostructure in transverse (a1, b1) and longitudinal (a2, b2) sections

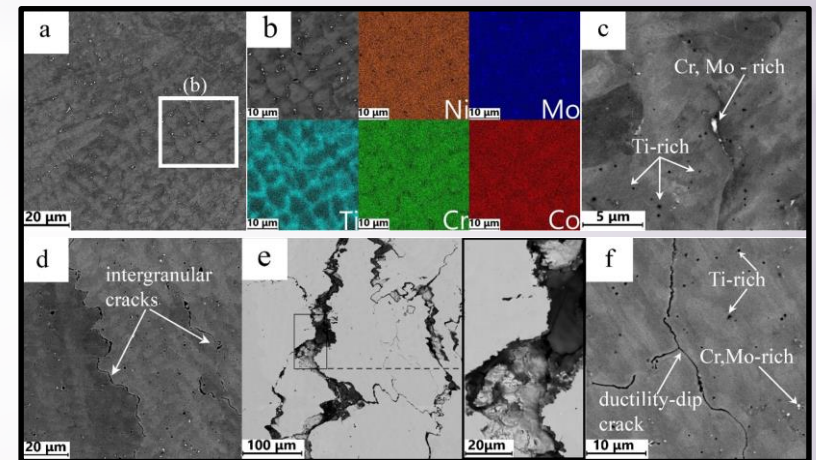
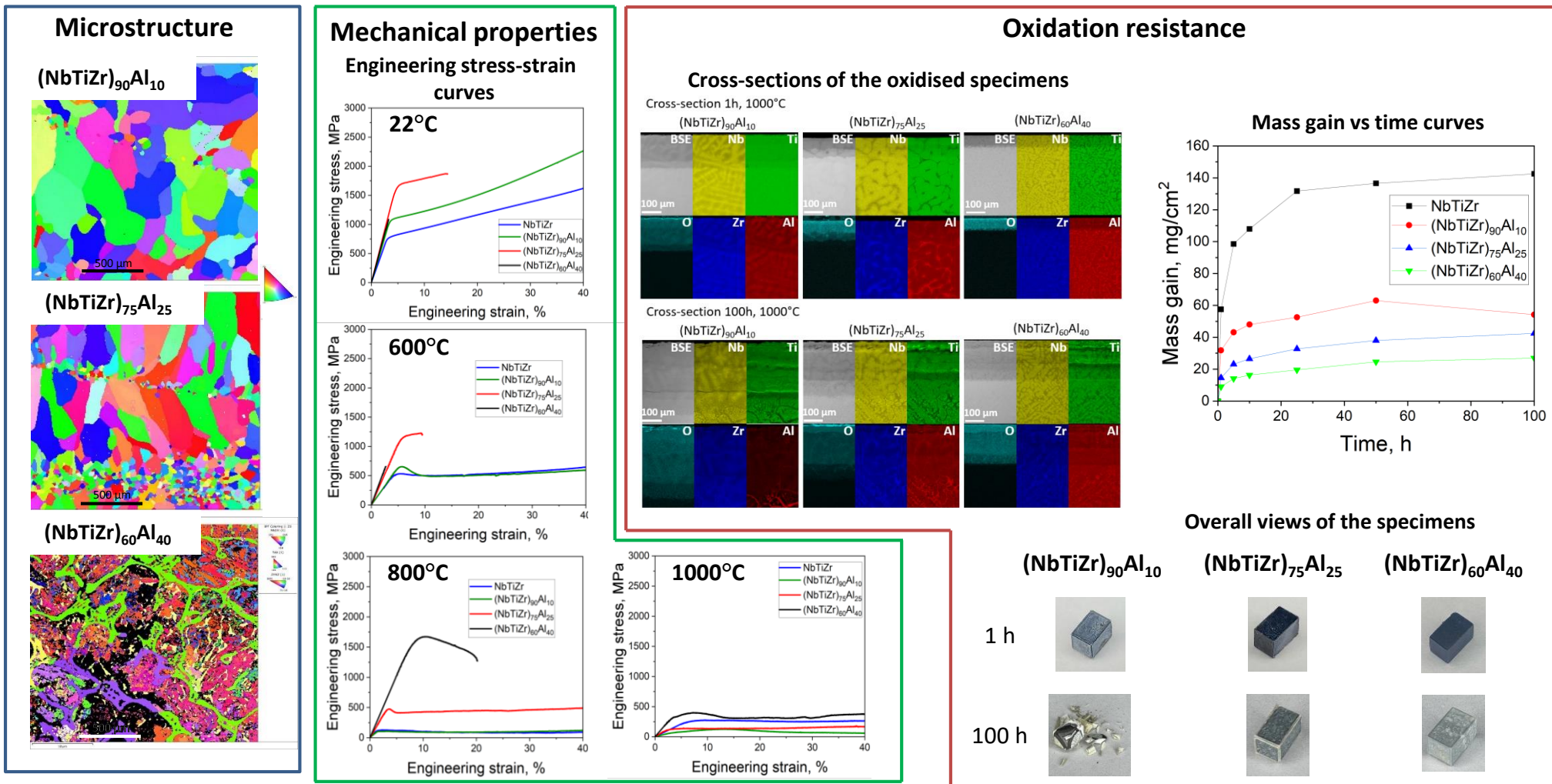


Figure 2. The SEM-BSE microstructure of the crack-free (a, b, c) and cracked (d, e, f) walls in the longitudinal section; Energy-dispersive spectroscopy (EDS) elemental mapping of dendritic structure (b).

*1387179@bsu.edu.ru

INVESTIGATION OF THE STRUCTURE, MECHANICAL PROPERTIES, AND OXIDATION RESISTANCE OF REFRACTORY MEDIUM-ENTROPY ALLOYS $Al_x(NbTiZr)_{100-x}$ (X= 10; 25; 40 at%)

M. A. Zhilina*, E. I. Nozdracheva, E. S. Panina, D. O. Kapustin, N. D. Stepanov, N. Yu. Yurchenko
Laboratory of Bulk Nanostructured Materials, Belgorod National Research University, Belgorod, Russia



evgeniaassanova@gmail.com

BCC-FCC PHASE TRANSFORMATION VIA HYDROGENATION OF THE ALLOYS IN Ti-V-Zr-Nb-Ta-Hf SYSTEM

Korol A.¹, Savvotin I.², Zadorozhnyy V.¹, Berdonosova E.², Zadorozhnyy M.^{1,3}, Assanova E.¹, Klyamkin S.²

1 National University of Science and Technology MISIS, Moscow, Russian Federation

2 Department of Chemistry, Lomonosov Moscow State University, Moscow, Russian Federation

3 Center for Project Activities of the Moscow Polytechnic University, Moscow, Russian Federation

Introduction

Feasibilities and characteristics a high-entropy non-equiatomic alloy of the composition $Ti_{0.25}Zr_{0.25}V_{0.15}Nb_{0.15}Ta_{0.20}$ was studied in this work. The samples for the investigation were created using the electron beam melting with pendant drop melt extraction (EBM-PDME). The first hydrogenation was carried out at room temperature by applying a thin layer of palladium to the sample. X-ray diffraction (XRD) was used to characterize the ongoing phase transformations of the alloy. The behavior of the alloy during its hydrogenation and dehydrogenation was studied using the volumetric method.

Results

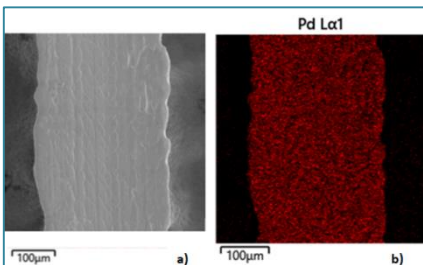


Fig. 1. The appearance of $Ti_{0.25}Zr_{0.25}V_{0.15}Nb_{0.15}Ta_{0.20}$ fibers obtained by EBM-PDME (a) and elemental (palladium) mapping (b).

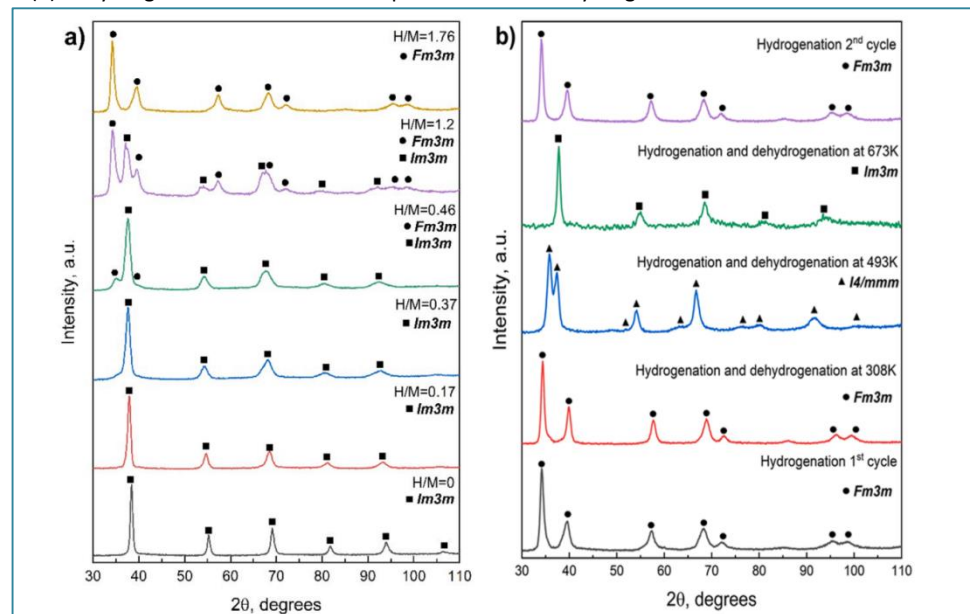
Thickness of the layer was amounted to about 240 nm. The total palladium content in the sample of less than 1 % so Pd phase is not detected.

Table 1. Phase composition and structure parameters of $Ti_{0.25}Zr_{0.25}V_{0.15}Nb_{0.15}Ta_{0.20}$ alloy and its hydrogenation products.

Sample H/M	Phase content, % at.	Cell parameter, nm	Space group	V_c , nm ³	$\Delta V/V^0$, %
0	100	a=0.3328(1)	Im(-)3m	0.0369	-
0.17	100	a=0.3353(1)	Im(-)3m	0.0377	2.2
0.37	100	a=0.3366(1)	Im(-)3m	0.0381	3.5
0.46	90	a=0.3379(1)	Im(-)3m	0.0386	4.7
	10	a=0.4465(1)	Fm(-)3m	0.0890	20.8
1.2	45	a=0.3421(1)	Im(-)3m	0.0400	8.6
	55	a=0.4560(1)	Fm(-)3m	0.0948	28.6
1.76	100	a=0.4558(1)	Fm(-)3m	0.0947	28.5
After dehydrogenation:					
At 308 K	100	a=0.4519(1)	Fm(-)3m	0.0923	25.1
At 493 K	100	a=0.3374(1) c=0.3713(1)	I4/mmm	0.0423	14.5
At 674 K	100	a=0.3341(1)	Im(-)3m	0.0373	1.1
Hydrogenation, 2 nd cycle	100	a=0.4551(1)	Fm(-)3m	0.0943	27.7

Results

Fig. 2. XRD-patterns of the $Ti_{0.25}Zr_{0.25}V_{0.15}Nb_{0.15}Ta_{0.20}$: (a) different stages of hydrogenation; (b) dehydrogenation at different temperatures and 2nd hydrogenation.



Conclusions

Until a hydrogen concentration of 0.46 H/M, the cell parameter of a single-phase BCC alloy increased from 0.3328 to 0.3366 nm. Then, a small amount of the FCC phase (a=0.4465 nm) appeared, increasing with further hydrogenation. The cell parameters of both BCC and FCC phases also increased. The completion of hydrogenation occurred at 1.76 H/M and the BCC phase disappeared. It is worth noting that a new orthorhombic I4/mmm phase was formed after dehydrogenation at 493 K.

maxsimpolykovv@gmail.com

Influence Of Magnetron Sputtering Regimes On The Structure And Properties Of Thin High Entropy Films CoCrFeNiCu

M.V. Poliakov, A.S. Rogachev

Merzhanov Institute of Structural Macrokinetics and Materials Science, Russian Academy of Sciences (ISMAN), Chernogolovka, Russia

INTRODUCTION

The main requirements for resistive elements include high accuracy in resistance, controlled by temperature [1]. Pure metals have a positive temperature coefficient of resistance (TCR), around $4 \cdot 10^{-3} \text{ K}^{-1}$, so there's a search for alloys with a lower TCR. High-entropy alloys, consisting of five or more metals in equal or comparable concentrations, are of interest because they form distorted crystal structures, resulting in high resistance and low TCR. Research in thin-film high-entropy alloys has rapidly developed [2].

MATERIALS AND METHODS

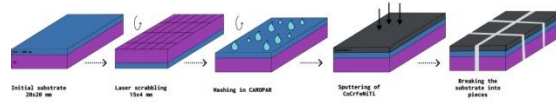


Figure 1 – Study preparation scheme

CONCLUSION

Figure 12 shows the HEA X-ray diffraction patterns of $\text{Co}_{0.22}\text{Cr}_{0.23}\text{Fe}_{0.29}\text{Ni}_{0.2}\text{Ti}_{0.06}$ thin films deposited at different sputtering time and power. The most intense peak in the XRD corresponds to FCC (111) with a cell parameter of 0.357 nm. The sputtering power for these thicknesses does not affect the structure, as the film was amorphous and remains so. The films have a smooth surface with a homogeneous distribution of elements (Figure 12b). The oxygen content of the films was evaluated by Auger spectroscopy and is not more than 4 at.% for all samples, except for the sample obtained at 100 W and 180 s, in this case the oxygen content is about 34 at.%.

The film composition (Figure 12b) at time deviates from the target composition not exceeding 1 at.%. Increasing the power from 100 to 1000 W at 720 s leads to a redistribution of elements: at 100 W the Cu content drops to 10 at.% due to oxidation, while at 1000 W Cu predominates. The optimum mode for accurate composition transfer is a power of 500 W and a time of 720 s.

By increasing the atomisation time from 180 to 720 s at 500 W power, the resistivity decreases from 820 to 34 $\mu\text{Ohm-cm}$ and TCR from -3000 to 140 $\text{ppm}/^\circ\text{C}$. As the crystallinity of the film increases, the conductivity increases. When the power is increased from 100 to 1000 W (at 720 sec), the resistivity varies from 23000 to 34 $\mu\text{Ohm-cm}$ and TCR from -800000 to 240 $\text{ppm}/^\circ\text{C}$. The difference is attributed to oxidation at 100 W. The optimum mode to obtain the minimum TCR is 500 W and 720 sec, with a resistivity of 34 $\mu\text{Ohm-cm}$ and TCS = 140 $\text{ppm}/^\circ\text{C}$.

The PF = 2.5 $\text{mW}/(\text{m} \cdot ^\circ\text{C}^2)$ value for the CoCrFeNiCu-based film obtained in this work is about 30 times higher than previously obtained for a similar system, and about 166 times higher than for the $\text{Co}_{0.22}\text{Cr}_{0.23}\text{Fe}_{0.29}\text{Ni}_{0.2}\text{Ti}_{0.06}$ composition. These results emphasise its significant potential as a thermoelectric and the need for further investigation of thermoelectric properties at higher temperature.

RESULTS

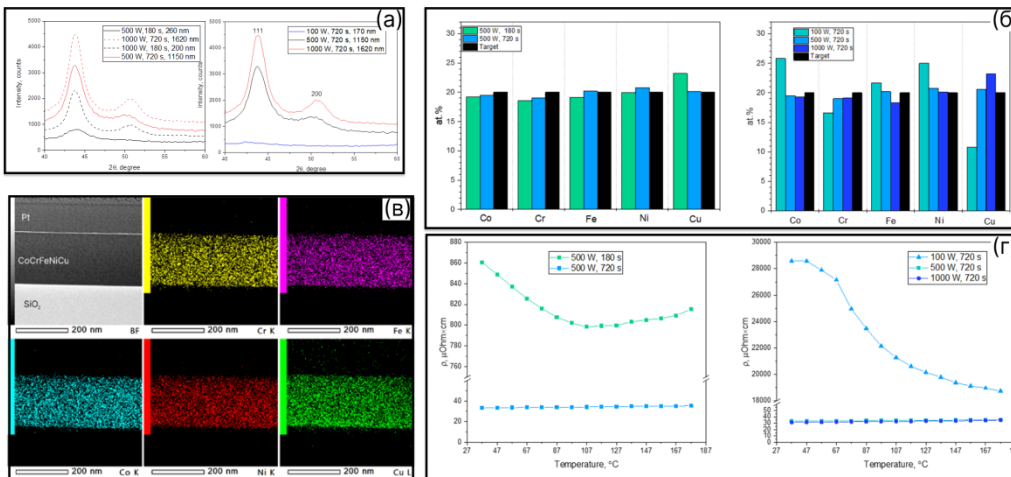


Figure 2 - Diffraction patterns (a), elemental composition (b), temperature dependences of resistivity from 37 to 177 $^\circ\text{C}$ (r) of HEA of CoCrFeNiCu thin films deposited at different sputtering time and power. SEM EDS cross-sectional mapping of CoCrFeNiCu HEA thin film obtained at 500 W and 180 s, thickness 260 nm (b)

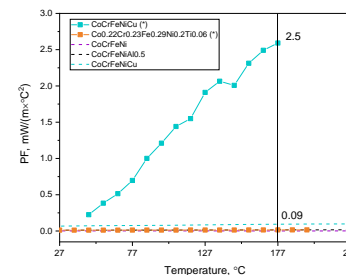


Figure 3 – PF-factor curve of CoCrFeNiCu and $\text{Co}_{0.22}\text{Cr}_{0.23}\text{Fe}_{0.29}\text{Ni}_{0.2}\text{Ti}_{0.06}$ thin films investigated in this work (marked with a star); CoCrFeNi, CoCrFeNiAl_{0.5} as well as CoCrFeNiCu in the temperature range from 27 to 227 $^\circ\text{C}$

ACKNOWLEDGMENTS

The work was supported by a grant from the Russian Science Foundation project no. 20-13-00277 P.

REFERENCES

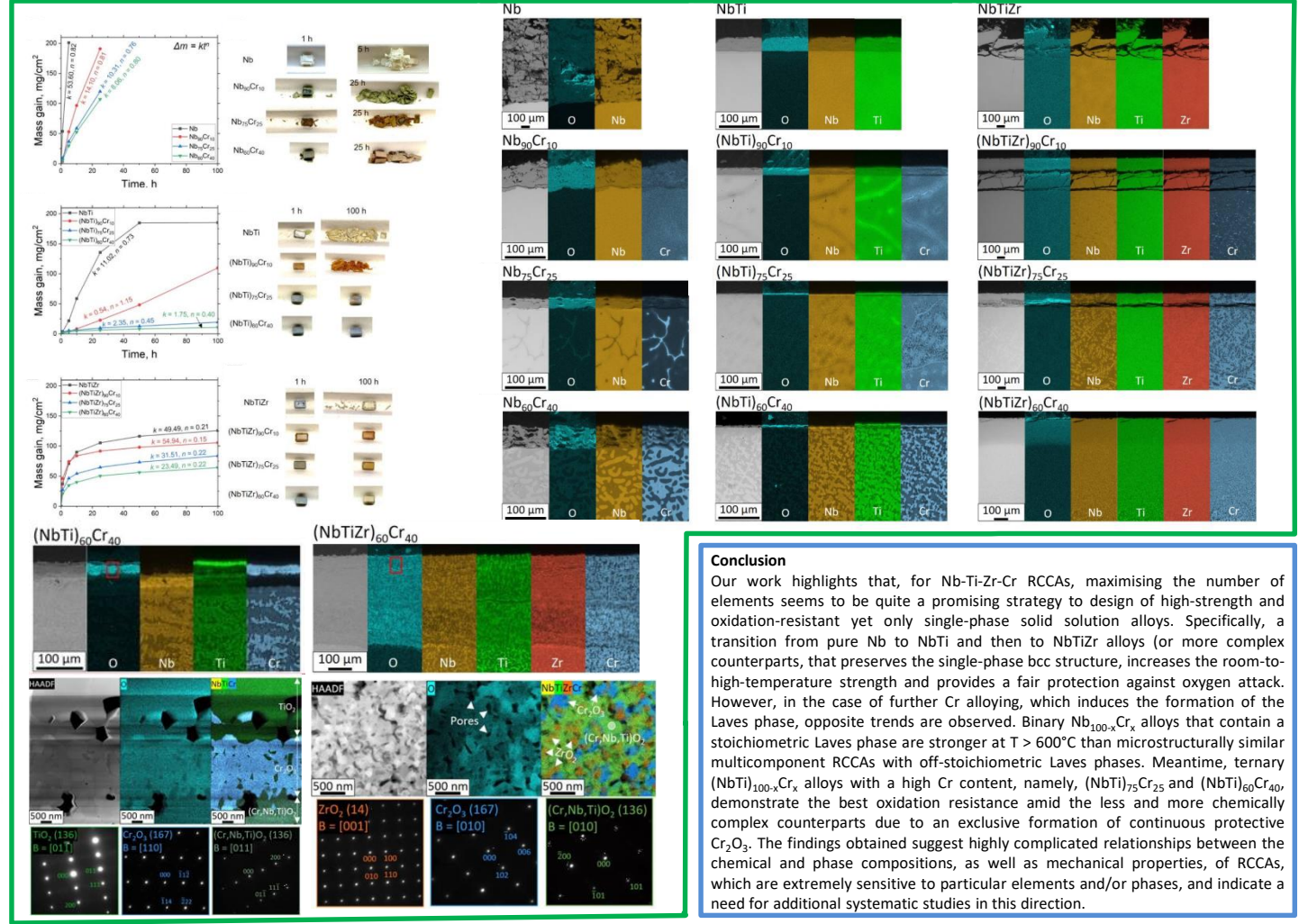
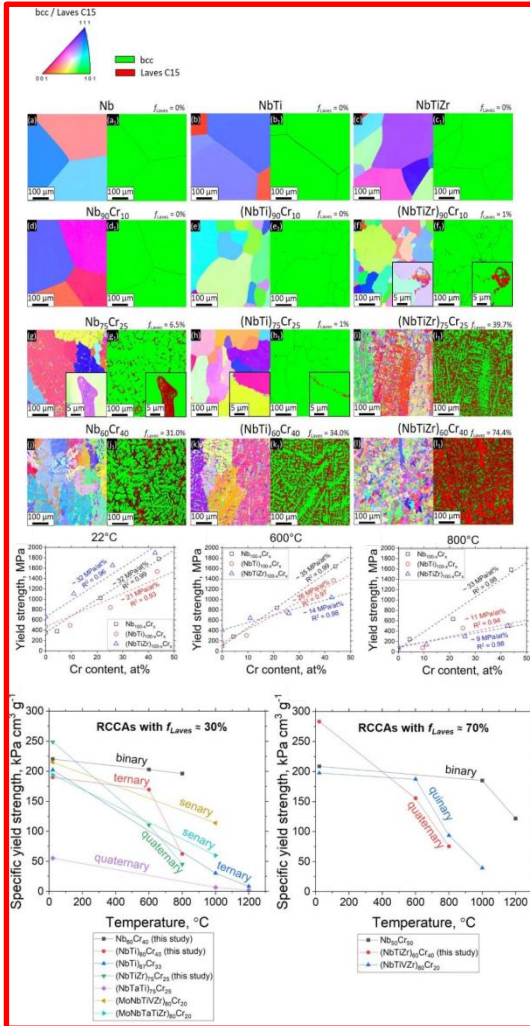
1. Matsuda K., Sato K., Doi T., Ogata K., and Konishi K., "Super precision metal film resistors," National Technical Report, vol.26, pp. 283–288, 1980.
2. Poliakov, M.; Kovalev, D.; Vadchenko, S.; Moskovskikh, D.; Kiryukhantsev-Korneev, P.; Volkova, L.; Dudin, A.; Orlov, A.; Goryachev, A.; Rogachev, A. Amorphous/Nanocrystalline High-Entropy CoCrFeNiTiX Thin Films with Low Thermal Coefficient of Resistivity Obtained via Magnetron Deposition. *Nanomaterials* 2023, 13, 2004, doi.org/10.3390/nano13132004.
3. Rogachev, A.S. Structure, Stability, and Properties of High-Entropy Alloys. *Phys. Met. Metallogr.* 2020, 121, 733–764, doi:10.1134/S0031918X20080098

*tuchina_k@bsu.edu.ru

STRENGTH AND OXIDATION RESISTANCE OF LAVES PHASE-CONTAINING REFRACTORY Nb-Ti-Zr-Cr ALLOYS: EFFECT OF CHEMICAL COMPLEXITY

Tuchina K. S., Kapustin D. O., Panina E. S., Stepanov N. D., Yurchenko N. Yu.

Laboratory of Bulk Nanostructured Materials, Belgorod National Research University, Belgorod, Russia



Conclusion
Our work highlights that, for Nb-Ti-Zr-Cr RCCAs, maximising the number of elements seems to be quite a promising strategy to design of high-strength and oxidation-resistant yet only single-phase solid solution alloys. Specifically, a transition from pure Nb to NbTi and then to NbTiZr alloys (or more complex counterparts, that preserves the single-phase bcc structure, increases the room-to-high-temperature strength and provides a fair protection against oxygen attack. However, in the case of further Cr alloying, which induces the formation of the Laves phase, opposite trends are observed. Binary Nb_{100-x}Cr_x alloys that contain a stoichiometric Laves phase are stronger at T > 600°C than microstructurally similar multicomponent RCCAs with off-stoichiometric Laves phases. Meantime, ternary (NbTi)_{100-x}Cr_x alloys with a high Cr content, namely, (NbTi)₇₅Cr₂₅ and (NbTi)₆₀Cr₄₀, demonstrate the best oxidation resistance amid the less and more chemically complex counterparts due to an exclusive formation of continuous protective Cr₂O₃. The findings obtained suggest highly complicated relationships between the chemical and phase compositions, as well as mechanical properties, of RCCAs, which are extremely sensitive to particular elements and/or phases, and indicate a need for additional systematic studies in this direction.

svetlana.degtyar3va@yandex.ru

POSITIVE EFFECT OF INCREASING THE QUENCHING TEMPERATURE ON THE CREEP RESISTANCE
 OF HIGH CHROMIUM STEEL WITH LOW NITROGEN AND HIGH BORON CONTENT

S.I. Degtyareva, A.E. Fedoseeva

Belgorod State National Research UniversitySt.
 Petersburg State Marine Technical University

Application

One of the promising materials for power unit components are martensitic steels with chromium content of 9-12%.

Main problem

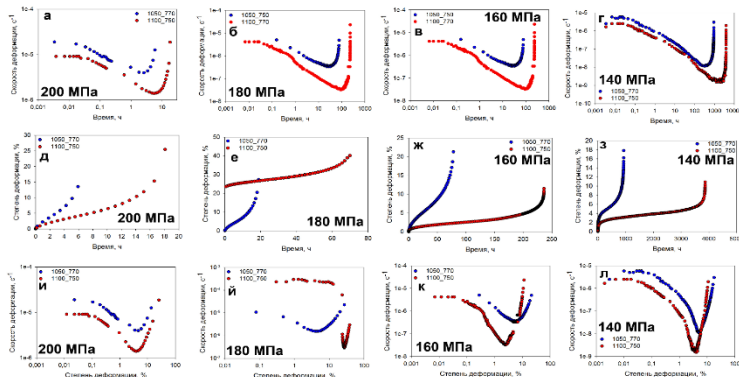
Low stability of the lath structure of martensite during creep at elevated temperatures.

Proposed solution

Apply a new modified heat treatment (1100°C+750°C) to isolate more secondary phases to harden the structure.

The aim of the present study: to reveal the effect of quenching temperature on the creep resistance of high chromium steel additionally alloyed with cobalt, tungsten, molybdenum and copper, with low nitrogen and high boron content.

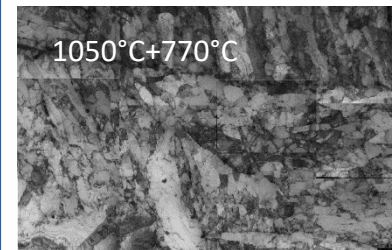
Creep properties



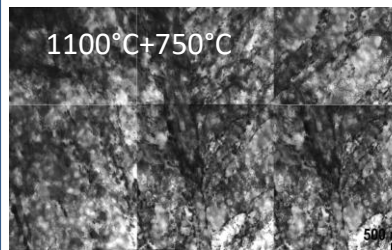
Graphs of time dependence of strain rate (a-g) and degree of deformation (d-h) as well as strain rate versus degree of deformation (i-l) at 650°C and applied stresses of 200 (a, d, i), 180 (b, e, j), 160 MPa (c, g, k) and 140 MPa (d, h, l)

The increase in time to failure was 3 to 4 times after application of 1100°C+750°C treatment. The minimum creep rate decreased by an order of magnitude at all applied stresses. Moreover, the slope of the long-term strength curve decreased from 0.083 after 1050°C+770°C treatment to 0.066 after 1100°C+750°C treatment.

Reference structure



933 h before destruction
 Rakes, nm: 640→890
 $\rho \cdot 10^{13} \text{ m}^{-2}$: 9→5
 Me_{23}C_6 : 50 nm → 79 nm
 MX: 27 nm → 40 nm
 Laves: 49 nm → 78 nm



3866 h before destruction
 Rakes, nm: 500→830
 $\rho \cdot 10^{13} \text{ m}^{-2}$: 6→4
 Me_{23}C_6 : 50 nm → 67 nm
 MX: 28 nm → 30 nm
 Laves: 47 nm → 101 nm